Elucidating severe urban haze formation in China

Song Guo[a,b], Min Hu[a,1], Misti L. Zamora[b], Jianfei Peng[a], Dongjie Shang[a], Jing Zheng[a], Zhuofei Du[a], Zhijun Wu[a], Min Shao[a], Limin Zeng[a], Mario J. Molina[c,1], and Renyi Zhang[a,b,1]

[a]State Key Joint Laboratory of Environmental Simulation and Pollution Control, College of Environmental Sciences and Engineering, Peking University, Beijing 100871, China; [b]Departments of Atmospheric Sciences and Chemistry, Center for the Atmospheric Chemistry and the Environment, Texas A&M University, College Station, TX 77843; and [c]Department of Chemistry and Biochemistry, University of California, San Diego, La Jolla, CA 92093

As the world's second largest economy, China has experienced severe haze pollution, with fine particulate matter (PM) recently reaching unprecedentedly high levels across many cities, and an understanding of the PM formation mechanism is critical in the development of efficient mediation policies to minimize its regional to global impacts. We demonstrate a periodic cycle of PM episodes in Beijing that is governed by meteorological conditions and characterized by two distinct aerosol formation processes of nucleation and growth, but with a small contribution from primary emissions and regional transport of particles. Nucleation consistently precedes a polluted period, producing a high number concentration of nano-sized particles under clean conditions. Accumulation of the particle mass concentration exceeding several hundred micrograms per cubic meter is accompanied by a continuous size growth from the nucleation-mode particles over multiple days to yield numerous larger particles, distinctive from the aerosol formation typically observed in other regions worldwide. The particle compositions in Beijing, on the other hand, exhibit a similarity to those commonly measured in many global areas, consistent with the chemical constituents dominated by secondary aerosol formation. Our results highlight that regulatory controls of gaseous emissions for volatile organic compounds and nitrogen oxides from local transportation and sulfur dioxide from regional industrial sources represent the key steps to reduce the urban PM level in China.

pollution | $PM_{2.5}$ | China | nucleation | secondary aerosols

Fine particulate matter smaller than 2.5 μm ($PM_{2.5}$) represents a major environmental problem, degrading visibility, negatively affecting human health, and directly and indirectly impacting weather and climate (1–5). Aerosols can be directly emitted (primary) or formed through the gas-to-particle conversion process (secondary) in the atmosphere (6, 7). The primary aerosol sources include emissions from combustion, road or wind-blown dust, and plants, while the secondary formation processes include nucleation and growth by multiphase chemical processes. Also, primary and secondary particles undergo chemical and physical transformations and are subjected to cloud processing and transport in the atmosphere (8, 9). The formation mechanisms leading to severe haze episodes with exceedingly high $PM_{2.5}$ levels in China remain highly uncertain, and the abundance and chemical constituents of $PM_{2.5}$ vary considerably, depending on complex interplay between meteorology, pollution sources, and atmospheric chemical processes (10–16). For example, on the basis of ambient measurements and receptor model analysis, the contribution to the annual mean $PM_{2.5}$ in Beijing has been suggested to be mainly from industrial pollution and secondary inorganic aerosol formation, but negligibly from traffic emissions (14). In addition, meteorological conditions may govern regional and long-range transport of air pollutants (17, 18).

Results and Discussion

$PM_{2.5}$ Episodes. We evaluated the contributions of secondary formation vs. primary emissions and local production vs. regional transport to the $PM_{2.5}$ levels in Beijing on the basis of measurements of ambient gases and aerosol properties. Since measurements at a fixed site (Fig. S1) may be affected by transport, local emissions, and chemistry, the evolutions of the particle size,

mass, number concentration, chemical composition, and meteorological parameters (such as measured wind direction and speed and back-trajectories) were analyzed to decouple the various processes. The measured $PM_{2.5}$ properties from 25 September to 14 November 2013, representative of the typical fall conditions in Beijing, exhibit a clear periodic cycle of 4–7 d. The measured particle mass concentration (Fig. 1A) reveals that the $PM_{2.5}$ level is less than 50 μg·m^{-3} (clean) in the beginning of each cycle, but reaches several hundred micrograms per cubic meter (polluted) within 2–4 d. The measured particle size distributions (Fig. 1B) demonstrate the presence of a higher number concentration of smaller particles during the clean period but a slightly lower particle number concentration of larger particles during the polluted period. The mean particle diameter (Fig. 1C) shows a similar cycle to that of the mass concentration (Fig. 1A). During the transition from the clean to polluted periods, an average daily particle mass growth of 50–110 μg·m^{-3} is accompanied by a daily increase in the mean diameter of 40–65 nm. The total particle number concentration exceeds 200,000 cm^{-3} during the clean period, and decreases slightly and remains at about 50,000 cm^{-3} as the pollution event develops (Fig. 1D).

During our observation period, southerly winds were most prevalent (50%), followed by winds from the northwest (42%) and northeast (7%) (Fig. S1). The wind was much weaker from the south but stronger from the northwest and northeast. The stronger northwesterly and northeasterly winds were most frequent during the clean period, carrying unpolluted air masses from the less populated northern mountainous areas. Furthermore, precipitation

Significance

We illustrate the similarity and difference in particulate matter (PM) formation between Beijing and other world regions. The periodic cycle of PM events in Beijing is regulated by meteorological conditions. While the particle chemical compositions in Beijing are similar to those commonly measured worldwide, efficient nucleation and growth over an extended period in Beijing are distinctive from the aerosol formation typically observed in other global areas. Gaseous emissions of volatile organic compounds and nitrogen oxides from urban transportation and sulfur dioxide from regional industry are responsible for large secondary PM formation, while primary emissions and regional transport of PM are insignificant. Reductions in emissions of the aerosol precursor gases from transportation and industry are essential to mediate severe haze pollution in China.

EARTH, ATMOSPHERIC, AND PLANETARY SCIENCES
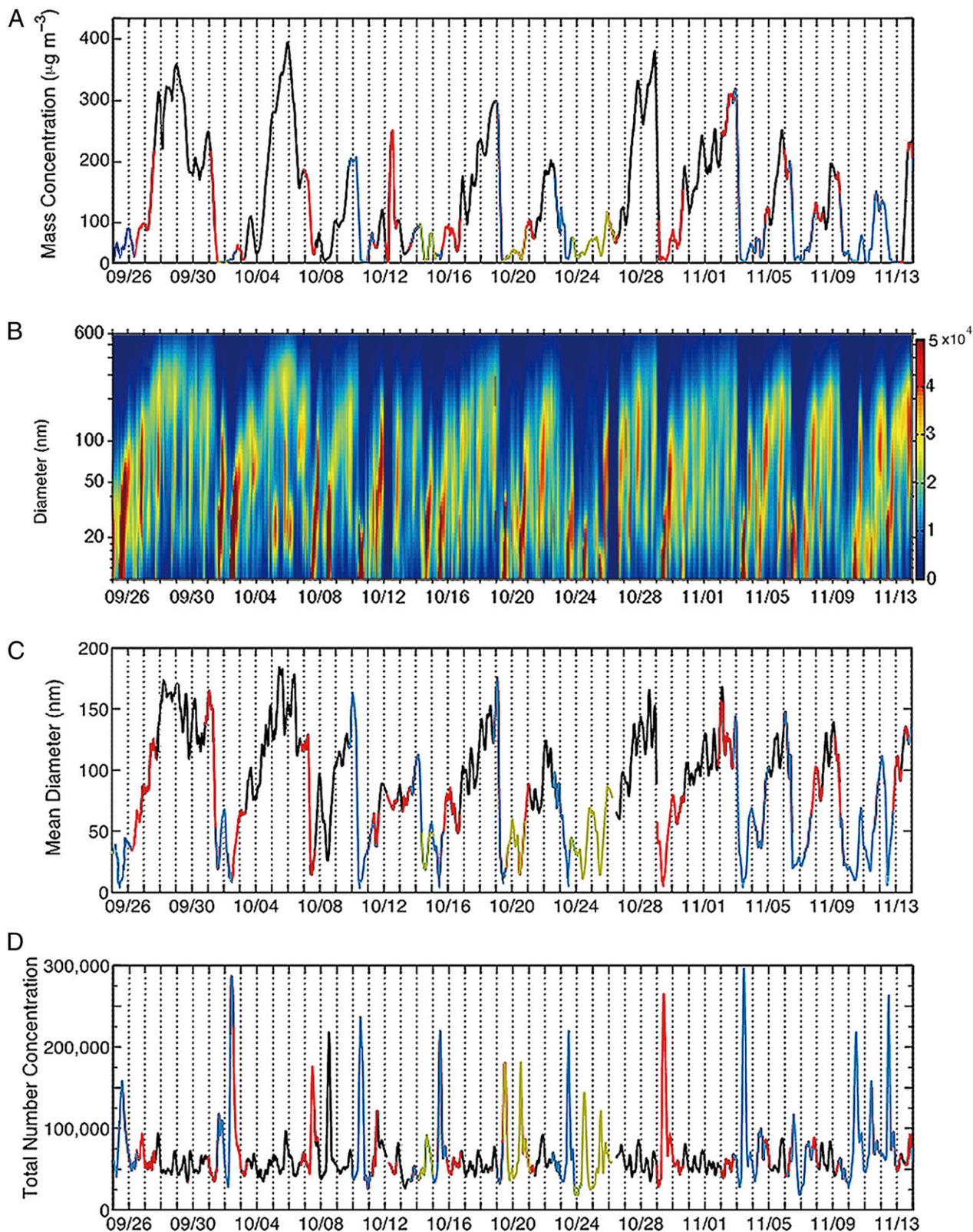
ENVIRONMENTAL SCIENCES

Fig. 1. Periodic PM$_{2.5}$ cycles in Beijing. Temporal evolutions of PM$_{2.5}$ mass concentration (*A*), number size distribution (*B*), mean diameter (*C*), and total number concentration (*D*) during the PM$_{2.5}$ events from 25 September through 14 November 2013. The colors in *A*, *C*, and *D* represent the air mass originating from the south (black), northwest (blue and red), and northeast (yellow), similar to those in Fig. S1. The color contour in *B* denotes the particle number concentration, i.e., dN/dlog$D$ (cm^{-3}) on the right vertical axis (where N and D represent the particle number and size, respectively). Each PM$_{2.5}$ cycle includes a clean period in the beginning, a polluted period in the end, and their transition. The dates on the *x* axis (also the vertical lines) correspond to midnight local time. The mean particle diameter is computed using a log-normal function from each measured size distribution at a given time.
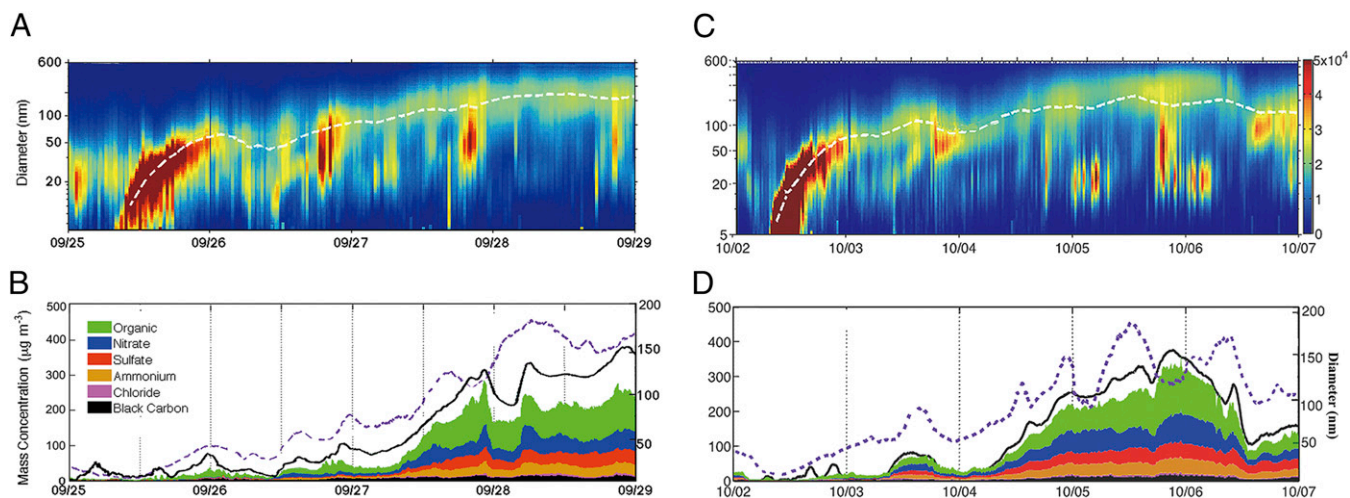
Fig. 2. Aerosol nucleation and growth during the PM$_{2.5}$ episodes on 25–29 September and 2–7 October. (*A* and *C*) Temporal evolutions of particle number size distribution and mean diameter (white dashed curve) on 25–29 September (*A*) and 2–7 October (*C*). (*B* and *D*) PM$_{2.5}$ mass concentration (black solid line), mean diameter (purple dashed line), and PM$_1$ (particulate matter smaller than 1.0 µm) chemical composition on 25–29 September (*B*) and 2–7 October (*D*). The shaded colors denote the mass concentrations of the aerosol constituents, i.e., green for organics, blue for nitrate, red for sulfate, yellow for ammonium, purple for chloride, and black for black carbon.

typically occurred between the pollution episodes, and wet deposition was also responsible for removal of aerosols. During the transition and polluted periods, the wind shifted from northerly to southerly with a considerably decreasing speed, resulting in air masses from the more populated southern industrial regions and a stagnant condition. The average mass concentrations of 35 µg·m^{-3}

and 114 µg·m^{-3} during the northerly and southerly wind conditions correspond closely to the clean and polluted periods, respectively. Hence, the wind variation correlates well with the PM$_{2.5}$ events (Fig. 1*A*), reflecting that the meteorological conditions represent one of the most critical parameters in regulating the cycles of pollution episodes in Beijing.
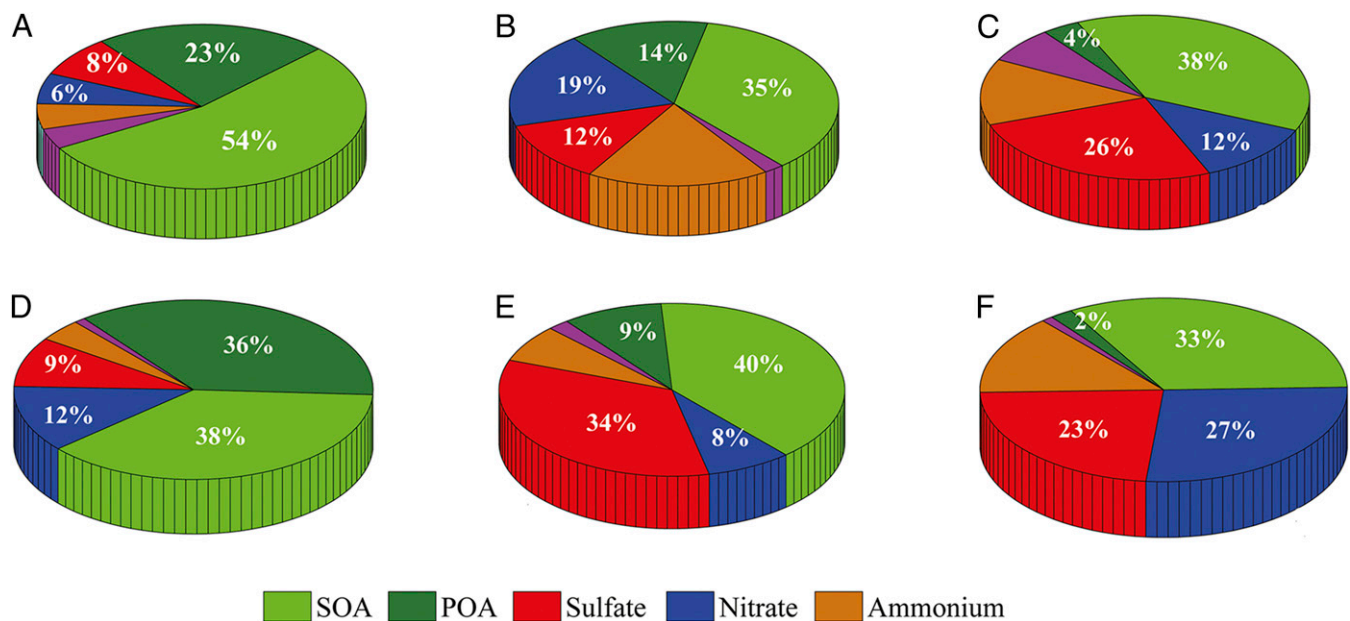

Fig. 3. Particle chemical compositions during the clean, transition, and polluted periods for the 25–29 September and 2–7 October episodes. (*A–C*) Chemical compositions for 80-nm (*A*), 100-nm (*B*), and 240-nm (*C*) particles measured by the AMS at 1500 h on 25 September, 1200 h on 27 September, and 1800 h on 28 September, respectively. The three particle sizes (i.e., close to the mean size) are selected to represent the dominant features in the chemical composition during the clean, transition, and polluted periods. At the three times, the hourly average PM$_{2.5}$ mass concentrations are 12 µg·m^{-3}, 167 µg·m^{-3}, and 288 µg·m^{-3}, and the particle mean diameters are 25 nm, 96 nm, and 151 nm, respectively. The mass concentrations of primary organic aerosols are 3 µg·m^{-3}, 14 µg·m^{-3}, and 13 µg·m^{-3} corresponding to *A*, *B*, and *C*, respectively, consistently small throughout the episode. (*D–F*) Chemical compositions for 80-nm (*D*), 100-nm (*E*), and 240-nm (*F*) particles at 1500 h on 2 October, 1200 h on 4 October, and 1200 h on 5 October, respectively. The hourly average PM$_{2.5}$ mass concentrations at the three times are 14 µg·m^{-3}, 111 µg·m^{-3}, and 312 µg·m^{-3}, and the particle mean diameters are 21 nm, 98 nm, and 192 nm, respectively. The numbers for the colors denote the mass concentrations of the aerosol constituents, i.e., light green for secondary organics, dark green for primary organics, blue for nitrate, red for sulfate, yellow for ammonium, and purple for chloride. The ammonium (yellow) mass fractions are 5% (*A*), 18% (*B*), 13% (*C*), 4% (*D*), 7% (*E*), and 14% (*F*), and the chloride (purple) mass fractions are 4% (*A*), 2% (*B*), 7% (*C*), 1% (*D*), 2% (*E*), and 1% (*F*).
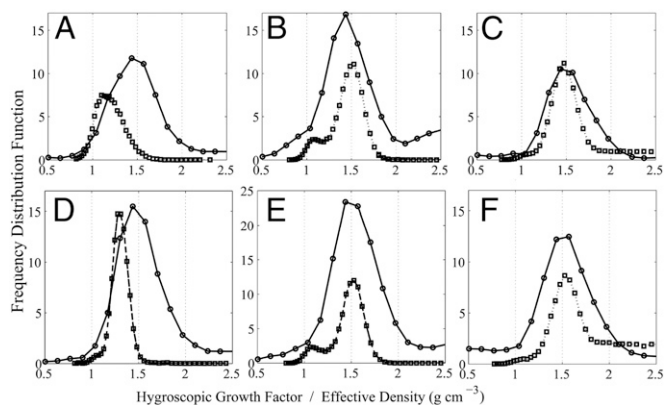
Fig. 4. Particle hygroscopicity and density during the clean, transition, and polluted periods for the 25–29 September and 2–7 October episodes. (*A*–*C*) Effective density (solid line, circles) and hygroscopicity (dashed line, squares) for 46-nm (*A*), 97-nm (*B*), and 240-nm (*C*) particles at 1500 h on 25 September, 1200 h on 27 September, and 1800 h on 28 September, respectively. (*D*–*F*) Effective density (solid line, circles) and hygroscopicity (dashed line, squares) for 46-nm (*D*), 97-nm (*E*), and 240-nm (*F*) particles measured at 1500 h on 2 October, 1200 h on 4 October, and 1200 h on 5 October, respectively.

The Aerosol Formation Mechanism. The processes governing the particle number and mass concentrations are further assessed by examining in detail the PM$_{2.5}$ events from 25–29 September and 2–7 October. During 25–29 September, for example, the development of the pollution episode includes two distinct secondary aerosol formation processes. The occurrence of high concentrations of nano-sized particles during the clean period is characteristic of aerosol nucleation (Fig. 2*A*). New particle formation typically corresponds to a regional event, and a variety of compounds have been associated with aerosol nucleation, including sulfuric acid, organics, basic species, and preexisting particles (7, 19–23). There is a noticeable absence of new particle formation as the pollution episode develops, indicating the suppression of nucleation by preexisting particles. During the transition and polluted periods, a continuous growth from the nucleation mode particles is clearly depicted by the evolution in the mean particle size (Fig. 2 *A* and *B*), which increases from about 40 nm when the PM$_{2.5}$ level is less than 50 µg·m^{-3} to about 190 nm when the PM$_{2.5}$ concentration exceeds 300 µg·m^{-3} over the course of 3 d. The largest increase of 270 µg·m^{-3} in the particle mass concentration occurs from 0600 h to 2200 h on 27 September, when the mean size increases by 63 nm. The fluctuation in the particle number concentration (Fig. 2*A*) is likely caused by coagulation, primary particle emissions, and wind speed and planetary boundary layer (PBL) variations. While the particle mass concentration is primarily sensitive to the fluctuations in wind speed and PBL height, the mean diameter is mainly influenced by primary particle emissions and coagulation. For example, the noticeably decreasing mass concentrations during the morning hours on 26, 27, and 28 September coincide with wind speed increasing by 1.8, 0.5, and 1.8 m·s^{-1}, respectively. Also, high concentrations of 30- to 100-nm particles are periodically observed during the morning and evening rush hours (Fig. 2*A*); the timing and size of the elevated aerosols are indicative of primary particle emissions originating from local transportation (24, 25). Although primary emissions by local traffic are clearly discernible by the transiently elevated number concentrations and may play a role in maintaining the particle number concentrations during the polluted period, these primary particles do not appreciably alter the particle mass growth. During the polluted period, the movement of the air mass is less than 50 km·d^{-1} estimated both from the measured wind speed and back-trajectory analysis, indicating a negligible impact from the regional PM$_{2.5}$ transport. Hence, the results depicted in Figs. 1 and 2 indicate that the aerosol nucleation and growth processes occur on the regional (several hundred kilometers) to urban (less than 100 km) scales, respectively, and local-scale phenomena, such as primary particle emissions by traffic, exert an insignificant impact on the particle mass growth.

Particle size and mass evolutions similar to those shown during the clean period (i.e., from 0900–2400 h on 25 September) have been commonly observed under diverse environmental conditions, including in pristine areas, and new particle formation produces a large fraction of the global aerosol population in the troposphere (7, 19–23). Typically, new particle formation and growth occur on a daily cycle in most regions worldwide (7), but few other locations exhibit particle growth as sustained and efficient as those displayed during the transition and polluted periods in Beijing (i.e., between 27 and 29 September in Fig. 2 *A* and *B*). It is also instructive to estimate the particle mass concentration on the basis of our measured particle size distribution and density: The calculated particle mass concentrations of 16 µg·m^{-3} and 380 µg·m^{-3} during the clean (1200 h on 25 September) and polluted (0000 h on 29 September) periods are in close agreement with the measured PM$_{2.5}$ values of 10 µg·m^{-3} and 360 µg·m^{-3}, respectively. Clearly, while the nucleation-mode particles (less than 30 nm) contribute negligibly to the particle mass concentration, the severe pollution episodes in Beijing are attributable to the presence of numerous large particles.

Additional analysis was performed for each pollution episode during our observation period (i.e., Fig. 2 *C* and *D* for the 2–7 October episode), showing consistently that nucleation produces high particle number concentrations in the beginning of a pollution cycle and that the development of a PM$_{2.5}$ event involves efficient and sustained growth from the nucleation mode particles over multiple days. Note that similar cycles in the variations of the particle mass concentration and size distribution (i.e., Fig. 1 *A* and *B*) are typical for other seasons in Beijing (11, 26, 27). For example, the frequency for the occurrence of new particle formation events is 50%, 20%, 35%, and 45% in the spring, summer, fall, and winter, respectively (11). In addition, a springtime periodic cycle of aerosol optical thickness and trace gaseous species (i.e., sulfur dioxide, carbon monoxide, nitrogen oxides, and ozone) has been previously identified at a rural site in northern China (28).

Measurements of the chemical composition by an aerosol mass spectrometer (AMS) (29) show continuously increasing mass concentrations of organics, sulfate, and nitrate during the episodes, correlating closely with the evolutions of the PM$_{2.5}$ mass concentration and mean particle size (Fig. 2 *B* and *D*). The organic mass fraction dominates in the clean period (74–77%) and decreases slightly during the transition (48–49%) and polluted (35–42%) periods (Fig. 3). The contributions of sulfate and nitrate to the particle mass concentration increase throughout the pollution period, with mass fractions of 8–9% and 6–12% for the clean period to 23–26% and 12–27% for the polluted period, respectively. Additional AMS-positive matrix factor analysis shows the secondary organic aerosol mass fraction is the largest, albeit decreasing slightly during the episode (i.e., from 38–54%, to 35–40%, to 33–38%). The primary organic aerosol mass fraction decreases considerably during the transition and polluted periods. The variation in the particle chemical composition is also reflected in the measured effective density and hygroscopicity (Fig. 4). During the clean period, the measured hygroscopic growth factor and effective density are both indicative of an organic-dominant composition, which is typically less hygroscopic and with a smaller density than the inorganic species (24, 25). In contrast, the increased hygroscopicity and effective density during the transition and polluted periods reveal the formation of internally mixed secondary organic and inorganic species, indicating increasing contributions from sulfate and nitrate. Evidently, there is a noticeable absence of the primary aerosol constituents from the hygroscopicity and density

measurements during the transition and polluted periods, including black carbon, primary organic aerosols, and mineral dusts, whose hygroscopicity and density characteristics are distinct from those of secondary organics and inorganic salts (24, 25). Furthermore, the AMS measurements reveal a non-negligible mass fraction of ammonium during the transition and polluted periods, which is also likely linked to automobile emissions (30). Hence, our analysis of the aerosol chemical composition indicates dominant secondary aerosol constituents throughout the episodes, i.e., the nucleation mode particles containing mainly secondary organics and $PM_{2.5}$ during the polluted period consisting primarily of secondary organics, sulfate, nitrate, and ammonium. Interestingly, while the evolutions in the particle size distribution and mass concentration for the severe $PM_{2.5}$ episodes in Beijing are noticeably distinct, the aerosol chemical compositions measured by AMS in our study are similar to those commonly measured in other global urban regions (29, 31–33). For example, the mass fractions of organic, sulfate, and nitrate measured by AMS are typically 45%, 23%, and 18% in urban regions worldwide (29, 31–33), comparable to the values of 43%, 17%, and 22% averaged over our entire measurement period in Beijing (Fig. 3), respectively.

The formation of the particle-phase organics, sulfate, and nitrate is attributable to emissions of volatile organic compounds (VOCs), sulfur dioxide (SO_2), and nitrogen oxides ($NO_x = NO + NO_2$), respectively (6, 7). Our gaseous measurements show highly elevated concentrations of these species during the pollution episodes (Fig. S2): The peak SO_2 and NO_x concentrations exceed 40 and 200 parts per billion (ppb), respectively, and the aromatic hydrocarbons (xylenes and toluene) represent the most abundant types of VOCs, with the peak xylene concentration exceeding 10 ppb (Fig. S2). Considering the relatively stagnant air mass (less than 50 km·d^{-1}) during the pollution periods and the atmospheric lifetimes (about 9.6 d for SO_2, 0.5–2.5 d for aromatics, and 1.0 d for NO_x) due to photooxidation by the hydroxyl radical (6), the SO_2 level in Beijing includes a large regional contribution transported from the southern industrial areas, but VOCs and NO_x are exclusively from local traffic emissions. Large particle mass growth (Fig. 1A) always occurs concurrently with elevated daily ozone concentrations (Fig. S2) throughout the $PM_{2.5}$ episodes, indicating the importance of photochemical activity in the secondary aerosol production. For example, the largest observed daytime (0600–1800 h) particle mass increases of 270 μg·m^{-3} on 27 September and 210 μg·m^{-3} on 4 October (Fig. 2 B and D) coincide with the elevated peak ozone concentrations of 110 ppb and 90 ppb, respectively. Photochemical oxidation and/or multiphase reactions of VOCs, SO_2, and NO_x in the atmosphere lead to formation of less volatile or nonvolatile species (34–36), contributing to the aerosol organic, sulfate, and nitrate constituents, respectively, in the nucleation and growth stages (6, 7, 37–40). Although the detailed aerosol chemistry leading to rapid PM mass growth in Beijing has yet to be elucidated, it is plausible that there exist synergetic effects among the various organic and inorganic compounds (i.e., organics, sulfate, nitrate, basic species, etc.) to enhance the particle growth (7, 20). Hence, our measurements of gaseous species provide additional evidence on the contribution of urban-scale photochemical production to the measured dominant secondary aerosol constituents, confirming small contribution from primary emissions and regional transport of $PM_{2.5}$. It should be pointed out that the pollution sources in Beijing are characteristic of the typical urban environments in China, i.e., with high emissions of VOCs and NO_x from local transportation and SO_2 from regional industrial sources (26, 27, 41, 42). Also, large contributions of VOCs and NO_x from local traffic and SO_2 from regional industrial sources to secondary aerosol production have been previously identified in other global megacity areas (31).

Conclusions

We have elucidated the coupling between meteorology, local emissions, and aerosol processes under extremely polluted conditions by conducting comprehensive atmospheric measurements. We show that the periodic cycles of severe haze episodes in Beijing are largely driven by meteorological conditions; stagnation typically develops with weak southerly wind from polluted industrial source regions, and precipitation represents an efficient removal mechanism for aerosols. The development of a pollution episode includes two distinct processes of aerosol formation, i.e., nucleation to initially produce high number concentrations of nano-sized particles and subsequently continuous growth from the nucleation mode particles. The combination of the enormously efficient aerosol nucleation and growth over an extended period (2–4 d or longer) yields a high mass concentration with numerous large particles during the severe $PM_{2.5}$ episodes in Beijing, uniquely different from those typically observed in other regions worldwide (7). On the other hand, the particle chemical compositions measured in Beijing are quite similar to those commonly measured in other global regions, consistent with the chemical constituents dominated by secondary aerosol formation (31, 33). Photochemical oxidation of VOCs and NO_x from urban traffic emissions and SO_2 from regional industrial sources is primarily responsible for the large secondary formation during the severe $PM_{2.5}$ events, but the contribution from primary emissions and regional transport of $PM_{2.5}$ is small. Considering the wide occurrence of new particle formation (7) and the similarities in the emission sources under typical urban environments, the mechanism of the efficient aerosol nucleation and growth leading to severe $PM_{2.5}$ development identified in Beijing is likely representative of other urban areas in China. Collectively, the urban areas and large city clusters, along with regional industrial facilities, agricultural activities, and biogenic emissions, throughout the country constitute the dominant sources of the regional $PM_{2.5}$ pollution in China.

From the mediation perspective, it is impractical to regulate new particle formation, but it may be feasible to intervene with aerosol growth processes to reduce $PM_{2.5}$ levels. Our results imply that reductions in emissions of aerosol precursor gases, i.e., VOCs and NO_x from transportation and SO_2 from regional industrial (such as power plants and manufacturing) sources, are critical for remediation of the severe urban and regional haze pollution in China. On the contrary, we suggest that an effort to solely control emissions of primary particles is unlikely to be effective. Since the formation of severe urban and regional haze in China is ultimately attributable to its rapidly growing economy, fast urbanization, and large population, leading to lower standards but higher rates for air pollutant emissions (41), regulatory measures by the Chinese government to reduce the $PM_{2.5}$ levels and to minimize its regional to global impacts (1–5) may have profound consequences on China or even the world economy.

Methods

The measurements were performed at an urban site located on the campus of Peking University in northwestern Beijing (11, 26, 27). A suite of state-of-the-art instruments was deployed to simultaneously measure comprehensive gaseous species and aerosol properties, including particle mass concentration, size distribution, chemical composition, density, and hygroscopicity (see also SI Text). Briefly, $PM_{2.5}$ mass concentrations were measured by a tapered element oscillating microbalance (TEOM). A combined nano-scanning mobility particle sizer (SMPS) and standard SMPS was deployed to measure the particle size distributions. The size-resolved particle density and hygroscopicity were measured using an aerosol particle mass analyzer and a hygroscopic tandem differential mobility analyzer (43–45). An Aerodyne high-resolution time-of-flight aerosol mass spectrometer was used to measure the chemical compositions of submicron particles, with a collection efficiency of about 50% (29, 46). Black carbon was measured by a single-wavelength (670 nm) Thermo multiangle absorption photometer.

1. Stocker TF, et al., eds (2013) *Intergovernmental Panel on Climate Change. Climate Change 2013: The Physical Science Basis. Contribution of Working Group I to the Fifth Assessment Report of the Intergovernmental Panel on Climate Change* (Cambridge Univ. Press, New York).
2. Wang Y, Zhang R, Saravanan R (2014) Asian pollution climatically modulates mid-latitude cyclones following hierarchical modelling and observational analysis. *Nat Commun* 5:3098.
3. Wang Y, et al. (2011) Long-term impacts of aerosols on precipitation and lightning over the Pearl River Delta megacity area in China. *Atmos Chem Phys* 11(23): 12421–12436.
4. Li Z, et al. (2007) Preface to special section on East Asian Studies of Tropospheric Aerosols: An International Regional Experiment (EAST-AIRE). *J Geophys Res* 112(D22): D22S00.
5. Wang Y, et al. (2014) Assessing the effects of anthropogenic aerosols on Pacific storm track using a multiscale global climate model. *Proc Natl Acad Sci USA* 111(19): 6894–6899.
6. Seinfeld JH, Pandis SN (2006) *Atmospheric Chemistry and Physics: From Air Pollution to Climate Change* (Wiley, New York).
7. Zhang R, Khalizov A, Wang L, Hu M, Xu W (2012) Nucleation and growth of nano-particles in the atmosphere. *Chem Rev* 112(3):1957–2011.
8. Zhang R, et al. (2008) Variability in morphology, hygroscopicity, and optical properties of soot aerosols during atmospheric processing. *Proc Natl Acad Sci USA* 105(30): 10291–10296.
9. Zhang R, Li G, Fan J, Wu DL, Molina MJ (2007) Intensification of Pacific storm track linked to Asian pollution. *Proc Natl Acad Sci USA* 104(13):5295–5299.
10. Sun Y, et al. (2014) Investigation of the sources and evolution processes of severe haze pollution in Beijing in January 2013. *J Geophys Res* 119(7):4380–4398.
11. Wu Z, et al. (2007) New particle formation in Beijing, China: Statistical analysis of a 1-year data set. *J Geophys Res* 112(D9):D09209.
12. Guo S, et al. (2013) Quantitative evaluation of emissions controls on primary and secondary organic aerosol sources during Beijing 2008 Olympics. *Atmos Chem Phys* 13:8303–8314.
13. Guo S, et al. (2012) Primary sources and secondary formation of organic aerosols in Beijing. *Environ Sci Technol* 46(18):9846–9853.
14. Zhang R, et al. (2013) Chemical characterization and source apportionment of $PM_{2.5}$ in Beijing: Seasonal perspective. *Atmos Chem Phys* 13(14):7053–7074.
15. Wang Y, et al. (2014) Mechanism for the formation of the January 2013 heavy haze pollution episode over central and eastern China. *Sci China Earth Sci* 57(1):14–25.
16. Wiedensohler A, et al. (2009) Rapid aerosol particle growth and increase of cloud condensation nucleus activity by secondary aerosol formation and condensation: A case study for regional air pollution in northeastern China. *J Geophys Res* 114(D2): D00G08.
17. Dickerson RR, et al. (2007) Aircraft observations of dust and pollutants over northeast China: Insight into the meteorological mechanisms of transport. *J Geophys Res* 112 (D24):D24S90.
18. Zheng GJ, et al. (2014) Exploring the severe winter haze in Beijing. *Atmos Chem Phys Discuss* 14(12):17907–17942.
19. Zhang R, et al. (2004) Atmospheric new particle formation enhanced by organic acids. *Science* 304(5676):1487–1490.
20. Zhang R, et al. (2009) Formation of nanoparticles of blue haze enhanced by an-thropogenic pollution. *Proc Natl Acad Sci USA* 106(42):17650–17654.
21. Zhang R (2010) Atmospheric science. Getting to the critical nucleus of aerosol for-mation. *Science* 328(5984):1366–1367.
22. Riccobono F, et al. (2014) Oxidation products of biogenic emissions contribute to nucleation of atmospheric particles. *Science* 344(6185):717–721.
23. Andreae MO (2013) Atmospheric science. The aerosol nucleation puzzle. *Science* 339(6122):911–912.
24. Levy ME, et al. (2013) Measurements of submicron aerosols in Houston, Texas during the 2009 SHARP field campaign. *J Geophys Res* 118(18):10518–10534.
25. Levy M, et al. (2014) Measurements of submicron aerosols at the California–Mexico border during the Cal–Mex 2010 field campaign. *Atmos Environ* 88:308–319.
26. Yue D, et al. (2010) The roles of sulfuric acid in new particle formation and growth in the mega-city of Beijing. *Atmos Chem Phys* 10(10):4953–4960.
27. Wang Z, et al. (2011) Evaluation on the role of sulfuric acid in the mechanisms of new particle formation for Beijing case. *Atmos Chem Phys* 11(24):12663–12671.
28. Li C, et al. (2007) In situ measurements of trace gases and aerosol optical properties at a rural site in northern China during East Asian Study of Tropospheric Aerosols: An International Regional Experiment 2005. *J Geophys Res* 112(D22):D22S04.
29. Aiken AC, et al. (2010) Mexico City aerosol analysis during MILAGRO using high resolution aerosol mass spectrometry at the urban supersite (T0) – Part 2: Analysis of the biomass burning contribution and the modern carbon fraction. *Atmos Chem Phys* 10(12):5315–5341.
30. Sun K, Tao L, Miller DJ, Khan MA, Zondlo MA (2014) On-road ammonia emissions characterized by mobile, open-path measurements. *Environ Sci Technol* 48(7): 3943–3950.
31. Molina LT, et al. (2010) An overview of the MILAGRO 2006 Campaign: Mexico City emissions and their transport and transformation. *Atmos Chem Phys* 10(18): 8697–8760.
32. Aiken AC, et al. (2009) Mexico City aerosol analysis during MILAGRO using high resolution aerosol mass spectrometry at the urban supersite (T0) – Part 1: Fine particle composition and organic source apportionment. *Atmos Chem Phys* 9(17):6633–6653.
33. Zhang Q, et al. (2011) Understanding atmospheric organic aerosols via factor analysis of aerosol mass spectrometry: A review. *Anal Bioanal Chem* 401(10):3045–3067.
34. Molina MJ (1999) Experimental study of intermediates from OH-initiated re-actions of toluene. *J Am Chem Soc* 121(43):10225–10226.
35. Zhang D, Zhang R, Park J, North SW (2002) Hydroxy peroxy nitrites and nitrates from OH initiated reactions of isoprene. *J Am Chem Soc* 124(32):9600–9605.
36. Zhao J, Zhang R, Misawa K, Shibuya K (2005) Experimental product study of the OH-initiated oxidation of m-xylene. *J Photochem Photobiol A* 176(1-3):199–207.
37. Zhao J, Levitt NP, Zhang R, Chen J (2006) Heterogeneous reactions of methylglyoxal in acidic media: Implications for secondary organic aerosol formation. *Environ Sci Technol* 40(24):7682–7687.
38. He H, et al. (2014) Mineral dust and NO_x promote the conversion of SO_2 to sulfate in heavy pollution days. *Sci Rep* 4:4172.
39. Wang Y, Zhang Q, He K, Zhang Q, Chai L (2013) Sulfate-nitrate-ammonium aerosols over China: Response to 2000–2015 emission changes of sulfur dioxide, nitrogen oxides, and ammonia. *Atmos Chem Phys* 13(5):2635–2652.
40. Zhao J, Levitt NP, Zhang R (2005) Heterogeneous chemistry of octanal and 2, 4-hex-adienal with sulfuric acid. *Geophys Res Lett* 32(9):L09802.
41. Wang M, et al. (2009) Use of a mobile laboratory to evaluate changes in on-road air pollutants during the Beijing 2008 summer Olympics. *Atmos Chem Phys* 9(21): 8247–8263.
42. He H, et al. (2012) SO_2 over central China: Measurements, numerical simulations and the tropospheric sulfur budget. *J Geophys Res* 117(D16):D00K37.
43. Khalizov AF, et al. (2009) Formation of highly hygroscopic aerosols upon internal mixing of airborne soot particles with sulfuric acid vapor. *J Geophys Res* 114(D5):D05208.
44. Khalizov AF, et al. (2013) Role of OH-initiated oxidation of isoprene in aging of combustion soot. *Environ Sci Technol* 47(5):2254–2263.
45. Pagels J, McMurry PH, Khalizov AF, Zhang R (2009) Processing of soot by controlled sulphuric acid and water condensation—Mass and mobility relationship. *Aerosol Sci Technol* 43(7):629–640.
46. He LY, et al. (2011) Submicron aerosol analysis and organic source apportionment in an urban atmosphere in Pearl River Delta of China using high-resolution aerosol mass spectrometry. *J Geophys Res* 116(D12):D12304.